Interfacial heat transfer with non-condensable gas in ASTEC V2.2: Application to severe accidents study during PWR cold shutdown states

Julie-Anne Zambaux, Laurent Laborde

INTERFACIAL HEAT TRANSFER WITH NON-CONDENSABLE GAS IN ASTEC V2.2: APPLICATION TO SEVERE ACCIDENTS STUDY DURING PWR COLD SHUTDOWN STATES

J-A. Zambaux[1], L. Laborde[1]

[1] Institut de Radioprotection et de Sûreté Nucléaire (IRSN), PSN-RES, Cadarache, 13115 Saint-Paul-lez-Durance, France

julie-anne.zambaux@irsn.fr, laurent.laborde@irsn.fr

Abstract

In a diphasic flow, the presence of non-condensable gas has an important impact on interfacial heat transfer, especially at low global pressure. In severe accidents studies, such flow can be commonly encountered. For example, in pressurised water reactors, high concentration of non-condensable gas can be found in the reactor coolant system in case of late core reflooding with a high oxidation rate (high hydrogen concentration) or in case of accidents happening during the cold shutdown of the reactor, when the reactor coolant system has been partly drained (high air concentration). Such flows with non-condensable gas are challenging to compute for severe accident system codes. A new model is implemented in ASTEC v2.2 to improve the interfacial heat transfer calculation in presence of non-condensable gas. The model gives a more accurate estimation of the heat transfer by assuming that it is mainly driven by vapour diffusion in the gas phase. The new model is applied to study cold shutdown states for 1300 MWe pressurized water reactors. A complete calculation of the cooling, depressurisation and draining of the reactor can be successfully performed. In order to show ASTEC new capabilities, a first accident scenario with loss of the residual heat removal system is also presented.

1. Introduction

Heat transfer and subsequent phase change phenomena are deeply affected by the presence of non-condensable gas in the gas phase. This has first been evidenced by Othmer [1] who showed that steam condensation is highly decreased by the presence of a small amount of air. In his experimental work on wall condensation, the heat transfer coefficient on the wall is decreased by 50% by adding a volume fraction of air of 0.5%. Since then, many authors have studied this influence and shown that every non-condensable gas has a similar effect, as it is reported in Huang et al. review paper [2]. They also reported that the influence of non-condensable gas becomes stronger at low operating pressure. The effect of non-condensable gas on the heat transfer is generally explained by an extra resistance layer added at the interface, as stated by Ren et al.[3].

In nuclear safety analysis, and more importantly in the study of severe accidents, such flows are a common occurrence (as in most industrial processes implying diphasic flows). This is a crucial issue in nuclear installations such as spent fuel pools but also in nuclear power plants including pressurized water reactors (PWR). Such flows can be encountered for example in loss of coolant accident (LOCA), in case of late core reflooding after the degraded core has been fully oxidised. In that case, there is a high amount of hydrogen flowing in the gas phase. Another example concerns accidents happening during the cold shutdown of the reactor and more specifically during mid-loop operations, when the reactor has to be stopped and partly drained. Such operation occurs

regularly either for fuel rods changing or to perform maintenance operations for example on steam generators. Reaching the cold shutdown states involves the depressurisation and cooling of the coolant system. For mid-loop operations conditions, steam generators are completely drained. In that case, a diphasic flow with a lot of air in the gas phase is to be expected in the coolant system along with low pressure and low velocities. During this phase, the reactor core cooling is ensured by the residual heat removal system (RHR). Incidents can happen such as the loss of this RHR system and can lead to accident conditions. Due to the specific conditions attached to cold shutdown states and the unavailability of many safety devices, such kind of accidents must be thoroughly studied in safety analysis as stated in [4]. Still few studies either experimental [5] or numerical [6] concern this type of accidents but it is a growing issue. As stated by Aksan [7], system code results validity in cold shutdown conditions (with low pressure, low velocities and a lot of non-condensable gas) is yet to be demonstrated.

In the ASTEC code [8], the coolant system thermohydraulic is modelled by the CESAR module. In order to model flows with high non-condensable gas concentration, a crucial point is the accurate modelling of the interfacial heat transfer. Different kind of models can be found in the literature to take into account the presence of non-condensable gas for the interfacial heat transfer calculation. Huang et al. [2] give a thorough review of different modelling approaches, among which the diffusion layer model. Basis assumption for this approach is that the diffusion of the vapour in the gas phase is the interfacial heat transfer driving mechanism. Diffusion layer models have been extensively studied and use an iterative process to assess the liquid-gas interface temperature and corresponding interfacial heat transfer. Kageyama et al.[9] present the calculation method in detail for film condensation in vertical tubes. In the case of system codes, this approach has been used for example for the thermal-hydraulic in the containment modelling with MELCOR [10] or MARS [11]**Error! Reference source not found.**. In the reactor coolant system (RCS), in the CATHARE code, a model derived from this approach has also been developed for flow with moderate amount of non-condensable gas [12].

The present paper shows the implementation in the CESAR module of a new model for interfacial heat transfer for the flow in the reactor coolant system, based on the diffusion layer approach. The new model is then applied to perform primary calculations in cold shutdown states conditions with the ASTEC code.

2. Interface temperature model for ASTEC V2.2

2.1 Model description

The interfacial heat transfer in CESAR is calculated as the sum of the heat flux between the gas and the interface, and between the liquid and the interface. Both those heat fluxes can be approximated by the classical expression given in Equation (1). The subscript *i* stands for values at interface while *k* can be either *l* for the liquid phase or *g* for the gas phase. A_i is the interfacial area between the two phases and D is the flow characteristic length (usually the hydraulic diameter for flow in the coolant system) while V is the volume. T is the temperature, λ is the phase heat conductivity and Nu_{ki} is the flow Nusselt number. In CESAR, depending on the flow configuration, Nu_{ki} is evaluated through different correlations from the literature.

$$Q_{ki} = A_i \frac{\lambda_k Nu_{ki}}{D} (T_k - T_i) V \qquad (1)$$

To calculate this heat transfer accurately, the interface temperature T_i has to be determined. As stated in introduction, this temperature mainly depends on the vapour pressure at the interface. Hence this temperature can be written as $T_{sat}(P_{vi})$. Assessing the interfacial heat transfer correctly can thus be done by finding the vapour pressure value at the gas-liquid interface.

In CESAR default approach, the vapour pressure at the interface is assumed to be the same as the vapour pressure in the whole volume. This approach gives reasonable results for low non-condensable gas mass fraction, when the vapour pressure is close to the total pressure. However, when the non-condensable gas mass fraction increases, this approximation can be questioned. As ASTEC is a system code, large volumes are usually considered in CESAR and the vapour amount close to the gas-liquid interface can be expected to be quite different from the mean total vapour amount in the volume. Moreover, such an approach can lead to numerical stability problems: when there is close to no vapour in the gas phase and P_v is null, a corresponding saturation temperature close or even below $0°C$ can be calculated which will lead to property assessment issues in the code (and obviously results accuracy problems).

The new model implemented in CESAR proposes a better assessment of the vapour pressure at the interface by adopting a model based on the diffusion layer approach, as outlined in [2].

Under the assumption of no vapour accumulation at the interface, it can be written that there is a balance between all vapour mass fluxes received by the interface. The two main vapour mass fluxes at the interface are the vapour mass flux due to vaporization/condensation and the vapour mass flux by diffusion in the gas phase, as illustrated on Figure 1. Hence at the interface Equation (2) can be written:

$$\dot{m}_{vap/cond} = \dot{m}_{diff} \tag{2}$$

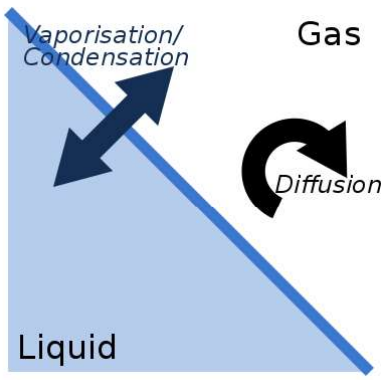

Figure 1 Vapour mass flux balance at the interface

Both these mass fluxes must be assessed at interface conditions. The vapour mass flux due to vaporization/condensation can be directly derived in Equation (3) from the interfacial heat transfer Q_i, expressed from the liquid and gas phase to interface heat transfers expressed in Equation (1), while L is the latent heat also calculated at the interface conditions.

$$\dot{m}_{vap/cond} = \frac{Q_i}{L} \quad (3)$$

The diffusion mass transfer in the gas phase is given in Equation (4). This mass flux is classically estimated from the flow Sherwood number Sh with a correction factor for suction effects of the boundary layer due to mass transfer. In that equation, ρ_g is the gas phase density and $\mathcal{D}$ is the vapour diffusion coefficient in the gas phase. V is the volume, while, as before, A_i is the interfacial area and D the flow characteristic length. f_v is the vapour molar fraction in the whole volume while f_{vi} is the vapour molar fraction at the interface. The Sherwood number compares diffusion and convection. Based on the heat and mass transfer analogy, Sh can be calculated using the same correlations as the one used for the Nusselt number in the corresponding flow conditions, by replacing the Prandtl number that compares viscous and thermal diffusivity ($Pr = \mu_g C_{pg}/\lambda_g$, with μ_g the gas dynamic viscosity and C_{pg} the gas heat capacity) by the Schmidt number that similarly compares viscous and mass diffusivity ($Sc = \mu_g/\rho_g\mathcal{D}$).

$$\dot{m}_{diff} = \rho_g \mathcal{D} Sh \frac{V A_i}{D} ln\left(\frac{1-f_v}{1-f_{vi}}\right) \quad (4)$$

In both Equations (3) and (4), the molar vapour fraction at the interface appears as the unknown (directly and through dependant parameters). In order to find this molar fraction, an iterative approach has to be adopted in order to satisfy Equation (2). Under the hypothesis that the gas mixture is ideal, vapour partial pressure at the interface can be deduced from this newly calculated molar fraction through $P_{vi}=f_{vi}P_{tot}$. Corresponding saturation and interfacial heat transfer terms can therefore be determined.

In CESAR, this new interface model has been implemented as an independent iterative loop performed at the beginning of each iteration of the Newton-Raphson method used by the CESAR solver. An additional dedicated Newton-Raphson scheme is used to reach a converged state. The output result is the molar fraction at the interface which can be used to calculate the interface temperature. Corresponding interfacial heat transfer is subsequently used during the main CESAR iterations.

2.2 Model effect analysis

In order to check the model effect, it is tested on a simple test case in which a single CESAR mesh is considered. The void fraction in the considered volume is *0.99*. The gas phase is a mix between vapour and a non-condensable gas, hydrogen in the present case. Initially, the amount of hydrogen is really low, with a molar fraction of *0.0001*. Both the liquid and the gas phase are at the same temperature $T_{sat(P_{tot})}$, close of the equilibrium. The volume is open with a fixed outlet pressure boundary condition at the top with a *1 m²* section. At the bottom, gas is injected at a fixed *1m/s* velocity through a *1 m²* section. As only H_2 is injected, it corresponds to an inlet mass flow rate of *0.064 kg/s*. The inlet gas is only hydrogen with total pressure and temperature conditions identical to the initial conditions. All the test case initial and boundary conditions are summed up on Figure 2. Volume considered is $1m^3$.

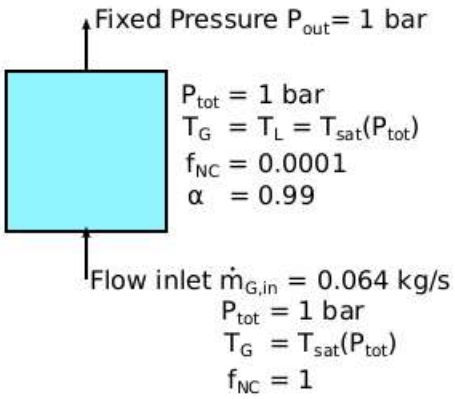

Figure 2 Test case initial conditions

In order to illustrate the effect of the new CESAR interface model, two calculations were performed. In the first one the default CESAR modelling is used while in the second one, the interface model is activated. Figure 3 presents the temperature evolution observed for the two calculations. Since the volume is open, the total pressure and the corresponding saturation temperature remain constant. The gas phase temperature is here controlled by the gas injection temperature. Hence, in both cases, gas temperature remains constant at the injection temperature (which is here the saturation temperature at total pressure).

As the vapour pressure decreases due to the hydrogen injection, the corresponding saturation also decreases. In both cases, this temperature reaches values very close to $0°C$. As stated before, the vapour amount decrease has an impact on the interface temperature which is expected to decrease also. The liquid phase will then become superheated and can be expected to vaporise. Hence the liquid phase temperature evolution in this test case is mainly driven by interfacial heat transfer and its equilibrium value is the interface temperature.

In the first calculation (default case), the interface temperature is the saturation temperature at vapour pressure. It can be seen on Figure 3(a) that the liquid phase temperature (in blue) decreases towards this saturation temperature at vapour pressure. However, some numerical limitations were introduced in the code to prevent calculating liquid temperatures too close to $0°C$, based on a direct convective-like heat transfer between gas and liquid. The liquid temperature stays around $7°C$ at minimum to avoid numerical problems due to water properties calculation from tables. This very simple test case illustrates arbitrary numerical limitations that had to be introduced in CESAR in order to avoid numerical problems due to a non-satisfactory modelling.

Figure 3(b) presents the results obtained when the new model is activated in CESAR. The interface temperature is now calculated using the interface vapour composition. The liquid temperature is equal to this new interface temperature in this case. The calculated interface temperature is considerably higher than the saturation temperature at vapour pressure which means that here the model estimates that the vapour concentration at the interface is higher than the global vapour concentration in the volume. It must also be noted that the interface temperature takes a longer time to reach its steady state. As long as there is still liquid that gets vaporised in the volume, the vapour composition at the interface keeps evolving here while the global vapour composition

remains quite unchanged due to the volume size (it should be reminded that in system codes similarly large volumes are usually considered).

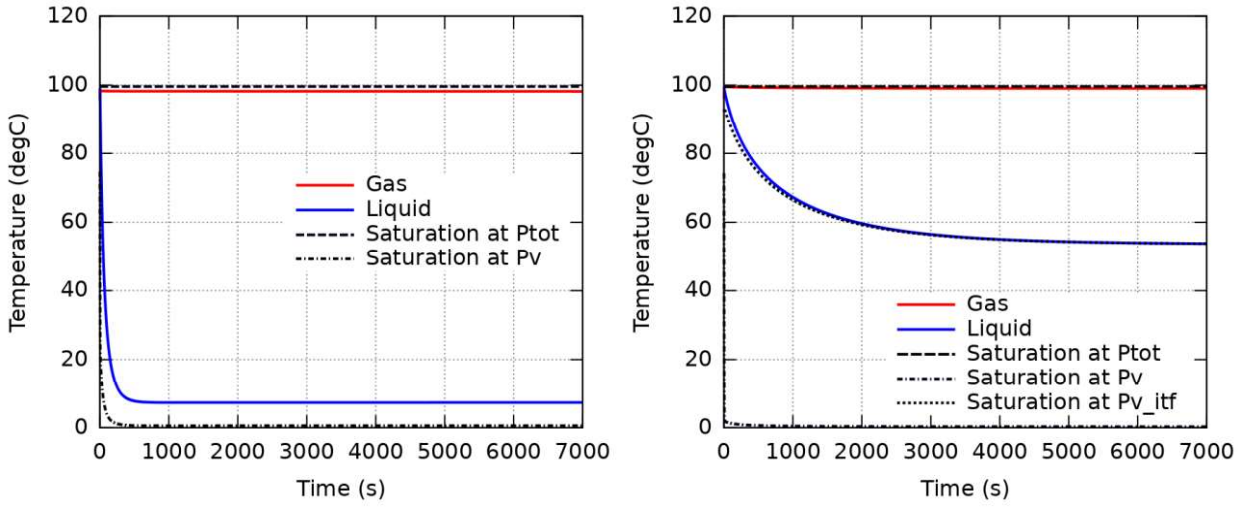

(a) Default ASTEC (b) Interface model activated in ASTEC

Figure 3 Comparison of the new interface model effect on the temperature evolution

The new model includes a new iterative loop and can be expected to affect the calculation time. Indeed, for reactor accident scenario analysis with system codes, calculation time is an important concern. On the very simple test case presented here with only one mesh and one ASTEC module is involved, no real analysis of the model impact on the calculation time can be made. First reactor scale calculations have shown that the model tends to increase the calculation time by few percent in general but also limits, in specific cases, the numerical issues due to problems in fluid properties calculations. In tested scenarios, the calculation time still remained reasonable (less than a week of calculation for a complete accident scenario calculation on a plant scale dataset). In the ASTEC v2.2 release, the new interface model is proposed as an optional model as it is still under study.

The test case presented here is a simple verification case that helps understanding why the model is needed and its effects. This is not however a validation study and it cannot be concluded that the new approach gives more accurate results (although they seem empirically more satisfactory). First validation elements are given in the next section.

2.3 Validation elements

ASTEC V2.2 with the new interface model is used to simulate analytic experiments that focus on specific flow regime and heat and mass transfer types often encountered in the calculation of PWR severe accident scenarios.

The first experiment considered is the COSI experiment and deals with direct vapour condensation during cold water injection in a horizontal pipe. A complete description of the facility is presented in [13]. Specific experiments in presence of nitrogen were performed at a working pressure around 20 bars. Initial conditions and experimental results are given in [12] and used to perform CATHARE simulations. The four cases presented in [12] are reproduced here in ASTEC v2.2

using the same modelling strategy. Table 1 sums up for each case, the initial conditions considered along with the experimental evaluated condensation mass flow rate $\dot{m}_{cond}$ and the one calculated by ASTEC v2.2. $\dot{m}_{g,in}$ is the gas mix mass flow rate while $\dot{m}_{l,inj}$ is the cold water injection mass flow rate. X_{N2} is the nitrogen mass fraction. As in what is shown experimentally, the presence of even a small amount of non-condensable gas visibly decreases the condensation.

Calculations were run for the four sets of initial conditions with and without the new interface temperature model activated. Results for both cases are given in Table 1. Globally the agreement between the experimental results and the numerical results seems quite satisfactory (as no experimental uncertainties are provided in [12]). Differences range from 5% to 20% with the model activated and from 5% to 25% without the model activated. It is worth noting that the new interface temperature model activation does only slightly improve the results.

Despite the high void fraction, the non-condensable gas mass concentration remains at most around 30% in these experiments. Results given by the new model remain quite close to the default model, which was expected as the default modelling (without the new interface model activated) is supposed to give valid results in these conditions. Higher non-condensable gas concentration than the ones considered experimentally should lead to a larger deviation between both models.

Run	P (bar)	$\dot{m}_{g,in}$ (g/s)	$\dot{m}_{l,inj}$ (g/s)	X_{N2}	$\dot{m}_{cond}$,exp (g/s)	$\dot{m}_{cond}$,calc (g/s) new model	$\dot{m}_{cond}$,calc (g/s) default model
1	23.3	170.	200.	0.	83.	88.	88.
2	21.8	180.	199.	0.094	72.	81.	80.
3	20.5	217.	198.	0.249	59.	69.	72.
4	22.	238.	199.	0.319	57.	69.	71.

Table 1 Comparison between the experimental results and the calculations for COSI with non-condensable gas

The second type of flow configuration considered concerns film condensation in a vertical pipe. Experiments performed in the presence of air by Tanrikut and Yesin [14] are used as they investigated flows with larger amount of non-condensable gas. A vertical counter-current exchanger is considered with a working pressure around 4 bars. Initial conditions of the chosen tests are presented on Table 2. A mix of steam and a varying mass fraction of air is injected downward at a total mass flow rate $\dot{m}_{g,in}$ in the inner pipe while coolant water at a mass flow rate $\dot{m}_{l,in}$ flows upward in the outer pipe. Geometrical data of the experiments are all extracted from [14]. Both the inner and the outer pipe are modelled in ASTEC. For the sake of simplicity, air is replaced by nitrogen in the simulations.

Run	P (bar)	$\dot{m}_{g,in}$ (g/s)	$\dot{m}_{l,in}$ (g/s)	X_{air}
1.4.1	3.96	27.	225.	0.
4.4.1	3.94	30.	231.	0.28
6.4.1	3.91	15.	253.	0.56

Table 2 Initial conditions for the film condensation simulation from [14]

In the experiments, temperature was measured in different positions using thermocouples including at the centre of the inner pipe, on the whole device length. These local measurements can be compared with the numerical results.

As stated in [14], the plotted centre line temperature value at 0 is the entrance gas temperature (that was also used in the calculations) while after, it corresponds to the interface temperature (a mixture of gas and liquid is expected at the centre of the exchanger), hence the decrease observed at the beginning of the experimental curve. The centre line temperature is thus compared with the interface temperature given by the new model and by the default model (assumed to be saturation temperature at the global volume vapour pressure in that case). Figure 4 presents the obtained results for the three sets of boundary conditions (on the Figure, dots correspond to the experimental results while the continuous lines correspond to the numerical results).

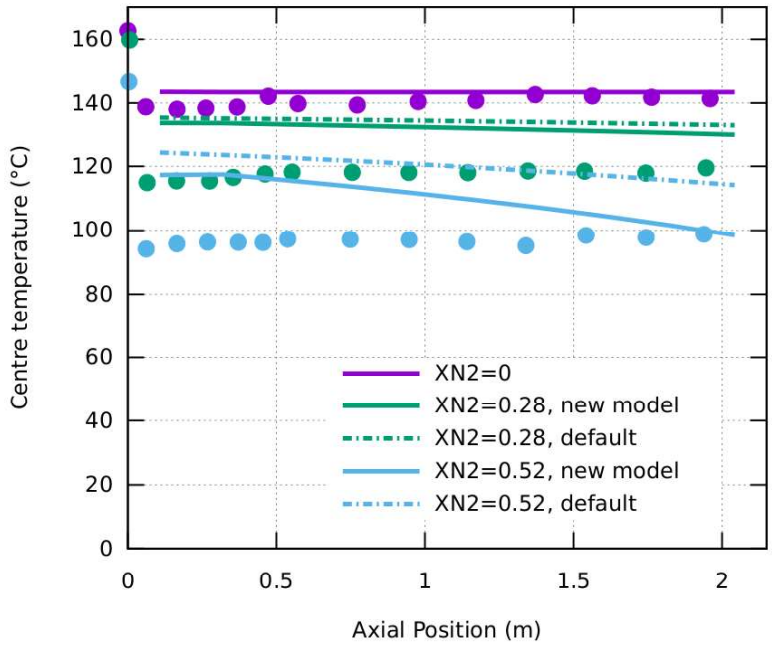

Figure 4 Comparison of the longitudinal temperature evolution for a vertical heat exchanger

On the numerical results, the experimental non-condensable mass fraction was used as the inlet condition. However, due to the vaporisation, this mass fraction increases along the tube length. Therefore, the interface temperature tends to decrease. On a qualitative point of view, the new interface model temperature gives a rather improved agreement with the experimental results. As observed previously, for the lower non-condensable mass fractions, both models give nearly the

same results, as the default model is still in its validity range. The increase of the non-condensable gas concentration leads to further difference in results between the two models. It is difficult to give a quantitative assessment of the modelling validity due to the rather large uncertainties on the experimental data (stated in [14]).

As it can be seen here, ASTEC v2.2 with the new interface model seems to give a good agreement with analytic scale experiments designed to study specific heat transfer configurations compared with results obtained with the default model, especially at higher non-condensable gas concentration values. Hence it can be seen that the new developed model gives satisfactory results. A more complete and extensive validation is still underway with also global scale experiments such as the analysis described in [15]. Nevertheless, it can already be used for specific calculations with high non-condensable gas amount which are numerically difficult to calculate with the default modelling such as mid-loop operation cold shutdown states.

3. Cold shutdown states calculation

3.1 Dataset and boundary conditions

In the calculations presented in this section, the equation system solved by CESAR is a classical two-fluid 6 equations system. A thorough description of CESAR 6 equation flow modelling can be found in [16], while validation elements are exposed in [17]. For complete plant calculations, CESAR is used along with ASTEC other modules. In the present calculation, the ASTEC modules used in addition to CESAR are ICARE for the in-vessel structures definition and heat transfer calculation (and core degradation calculation in severe accident scenarios), CPA for the containment thermal-hydraulic calculation and SOPHAEROS for fission product transport and inventory (see complete ASTEC code description in [8]). In the current paper, analysis and discussion will be focused on the CESAR module, coupled with ICARE for the vessel description.

The reactor type considered for this study is a French 1300 MWe pressurised water reactor with four steam generators and corresponding primary coolant system loops. A simplified visualisation of the ASTEC meshing for the reactor coolant system is presented on Figure 5. Secondary circuit is in green while the primary circuit is in blue. Only the first loop which is connected to the pressuriser is represented here for more clarity. In the dataset, the chemical and volume control system (CVCS), let-down and charging lines are not meshed but represented by boundary conditions.

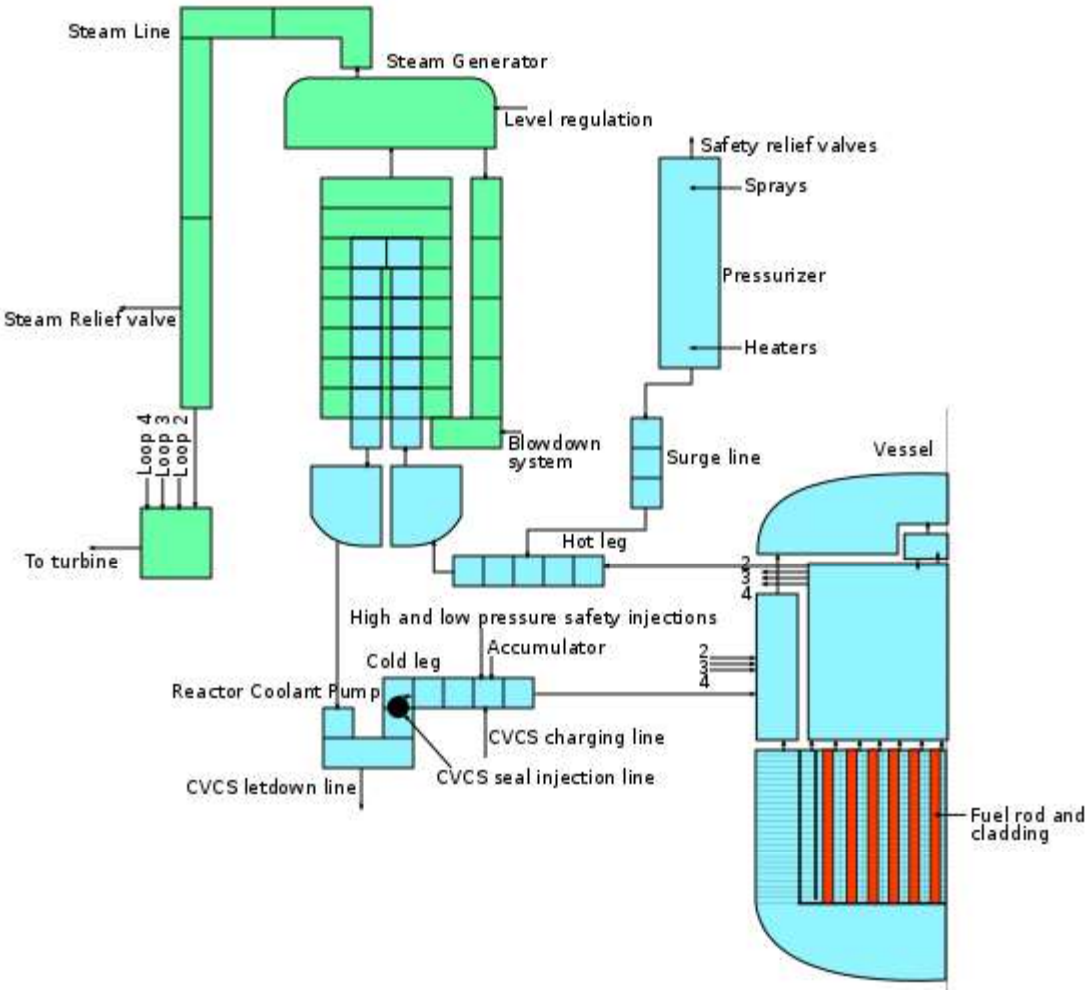

Figure 5 Mesh of the primary (in blue) and secondary (in green) coolant systems

To study cold shutdown states, the RHR system must also be taken into account in the dataset. On 1300 MWe PWRs this system is made of two symmetric parts each connected to two loops. Water is extracted from the hot leg of one loop, cooled and then reinjected in the cold leg of another loop. There is also a direct connection between the RHR system and the let-down line of the CVCS (boundary condition in the ASTEC dataset). Pressure regulation during cold shutdown or draining is achieved through this let-down line. Cooling is performed through an exchanger with the Component cooling water system (CCWS), which is supplied by the environment. A simplified representation of the RHR system is presented in blue on Figure 6 while the CCWS is in green.

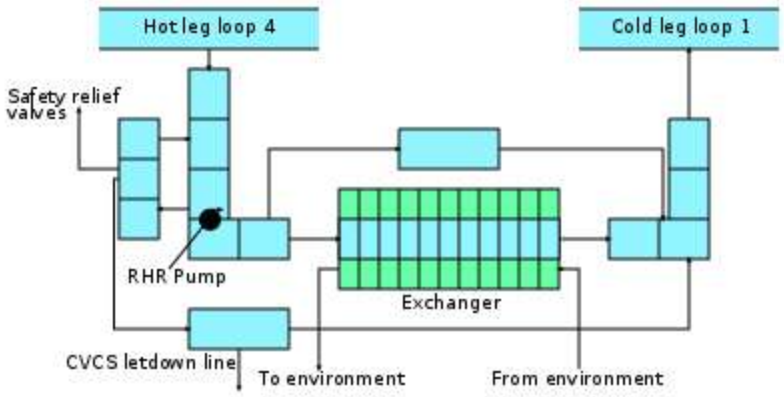

Figure 6 Simplified representation of the RHR system

3.2 Reaching cold shutdown states

In the frame of Probabilistic Safety Analysis of level 2 performed at IRSN, ASTEC is required to be able to compute accidents occurring at any instant of the cold shutdown process. Indeed, these scenarios represent a significant part of the most frequent accidents revealed by PSA level 2 studies Therefore, it is important to simulate with ASTEC the whole cold shutdown sequence. Initially, the reactor is taken at normal functioning conditions with *100%* nominal power (NP). In the primary coolant circuit, pressure is *155bar* while the temperature is *307°C*. Nominal power is then set to 0%. This is the so-called hot shutdown state (*P=155bar* and *T=297°C*). To reach cold shutdown states, both the pressure and temperature must be decreased. This must be done while remaining in a given pressure-temperature domain. Figure 7 shows the authorized pressure-temperature domain for the primary coolant system. At low pressure, the domain is limited at T_{sat}-*30°C* to ensure that the fluid remains in the liquid state. Additional limitations are also introduced to prevent thermal or pressure stress on components such as the pressuriser surge line or the steam generator tubes.

As it can be seen on Figure 7, when the pressure *P* is lower than *30bar*, steam generators can no longer be used to ensure an efficient heat removal and the RHR system has to be connected. From that point, the RHR system is ensuring the cooling, this system being qualified for pressure lower than *31bar*. Once the RHR is connected and temperature is further decreased, pressuriser is completely filled with water and pressure regulation is now ensured by discharge through the CVCS system. When the temperature is low enough, the primary pumps are stopped and the RHR system is thus the only one ensuring the flow circulation. Both the pressure and temperature can then be decreased till room conditions are achieved (cold shutdown state for intervention is reached for a primary system pressure below *5bar* and a temperature between *10°C* and *60°C* for 300We PWR).

Using ASTEC v2.2, it is possible to model the complete cold shutdown sequence using coded events to simulate the operator actions. On Figure 7, the blue line shows the calculation results (evolution of the primary circuit mean pressure and temperature). No particular calculation issue was detected during this phase.

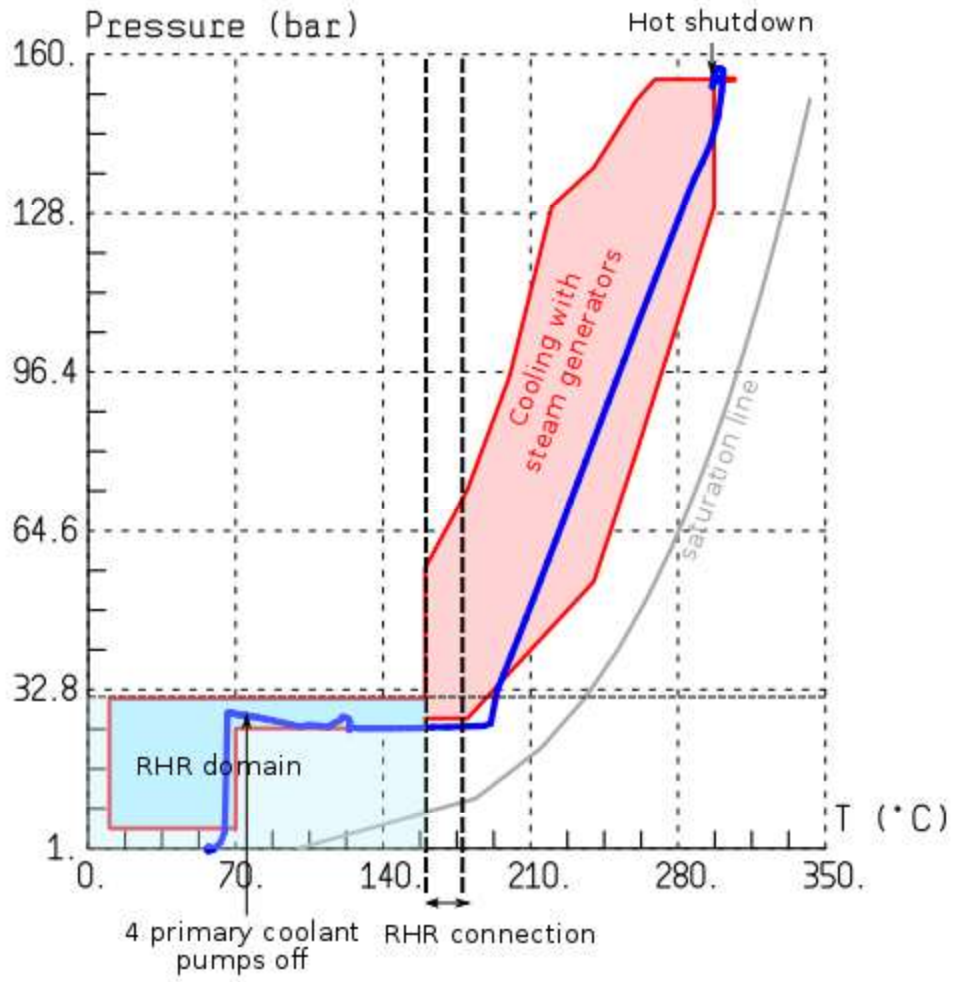

Figure 7 Pressure-Temperature domain for reaching cold shutdown states

In the frame of cold shutdown states studies, it is crucial to be able to calculate accident during mid-loop plant operations. In that case, the primary coolant circuit is opened (at both the pressuriser and the upper head of the vessel) and the water level is decreased till half of the cold and hot legs height. In that state, the steam generators are completely drained but there is still enough water in the primary loops to ensure that no gas is aspired into the RHR system (hence avoiding damaging the RHR pumps). This is a delicate part to simulate with system codes as flow becomes diphasic, stratified, with a gas phase mainly composed of air.

Using the new interface model developed for ASTEC v2.2, achieving that state can be done without calculations issues. In the calculation, only N_2 was considered instead of air to simplify the dataset. Liquid is discharged through the CVCS let-down line (see Figure 5) which is treated as a flow boundary condition. Discharge is stopped when the target liquid mass remaining inside the primary system is reached (chosen close from real plants data). In order to help replacing the

liquid by outside air, a N_2 mass flow source term is used in the vessel upper head and pressuriser. Moreover, a fixed outside pressure condition is also set on both volumes to ensure no pressure accumulation.

Figure 8 presents the evolution of the total fluid mass in the RCS and the pressure in the pressuriser. It can be seen from Figure 8(a) that the draining starts around *24h* after the reactor shutdown and is achieved after *36h*. During the draining phase, the total fluid mass in the RCS decreases as liquid water is replaced by air. The pressuriser is the first volume to be drained as one of the openings is located at its top. It can be seen on Figure 8(b) that as soon as the draining starts, the pressuriser gets completely filled with nitrogen.

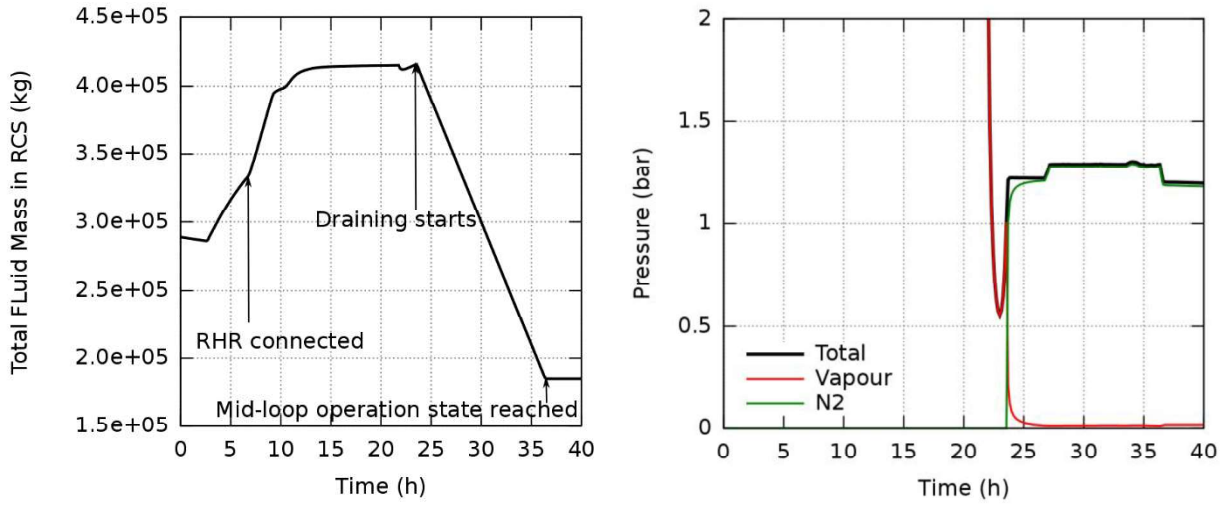

(a) RCS total fluid mass evolution (b) Pressure in pressurizer

Figure 8 RCS state during the cold shutdown of the reactor

It is difficult to assess the model gain in terms of accuracy since there is no comparison data as this is a global ASTEC reactor scale calculation. However, the gain in terms of numerical stability is obvious. With the new model, no temperatures below *0°C* were calculated during the draining phase which leads to a smoother fluid properties assessment. Hence the calculation can be performed in a reasonable calculation time (comparable with ASTEC v2.2 usual CPU time for reactor scale transient calculation).

3.3 First accidental configuration

A first feasibility study for accident calculations during cold shutdown states is performed. The scenario considered is a loss of the RHR system during mid-loop operations. As mentioned in the previous section, RHR system is the only system ensuring the fluid circulation (main coolant pumps of the primary circuit are all switched off) and cooling of the residual heat. In case of RHR loss, the fluid can heat up and this can lead to water vaporisation and subsequent core uncovery and degradation. The previous presented calculation is used for initiating the accident phase, starting 4 hours after the achievement of the mid-loop operation state (to ensure a steady state is reached). In this new calculation, RHR pumps are both stopped at the beginning of the sequence.

In this very simplified test sequence, the fixed pressure boundary conditions set during the discharge on the pressuriser and vessel upper head volumes remain active to model the fact that both volumes are open. To get a more realistic sequence, a connection should instead have been established between those volumes and the containment. This will be the case in future studies. No specific operator action is also modelled here as it is only a test sequence.

Figure 9 describes the evolution of the RCS behaviour during the accident. On the left, the evolution of the total fluid mass inventory in the RCS is plotted. It can be seen that after the RHR pumps are stopped, the total mass decreases as liquid is converted to vapour and temperature increases. Degradation of the core starts around *50h* and the vessel lower head fails around *70h*.

On the right of Figure 9, the evolution of the pressure in the pressuriser is presented. It can be seen that quite quickly the nitrogen present in the RCS is ejected outside and replaced by the generated vapour. Pressure increases till an equilibrium is reached between the vapour production and the mass flow rate at both fixed pressure outlet conditions set on the pressuriser and vessel upper head. Then, pressure increases drastically when the degradation starts as vapour production becomes more intense. At that point, hydrogen also starts appearing due to core oxidation.

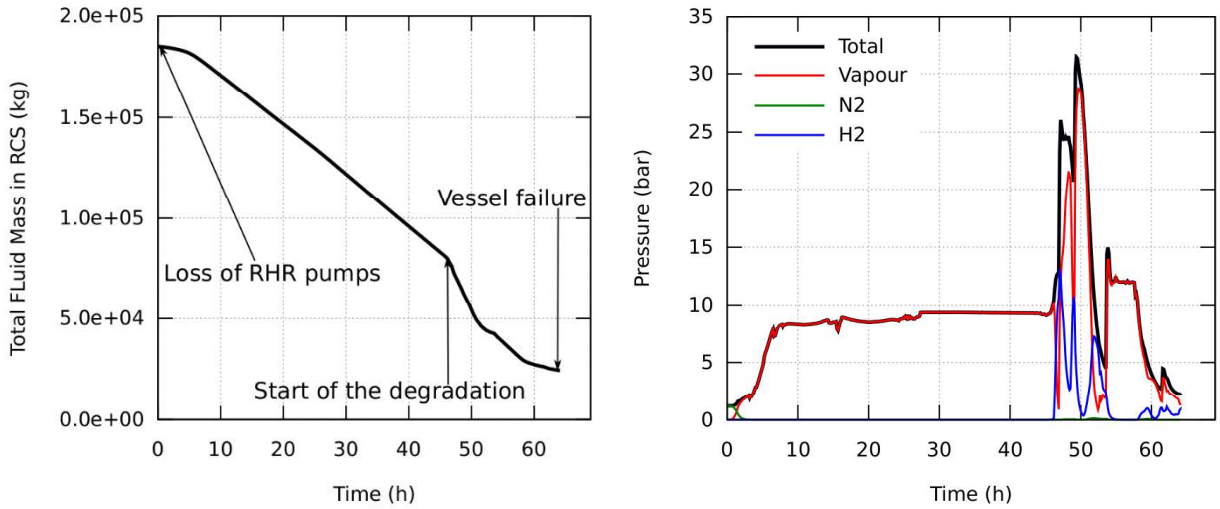

(a) Total fluid mass inventory (b) Pressure evolution in pressuriser

Figure 9 RCS behaviour during the accident

The whole accident calculation runs without crashes, for approximately 4 days which is not deemed excessive considering ASTEC usual calculation time for other kind of accident scenarios using the same meshing.

4. Conclusions

- A new model has been introduced in the ASTEC module CESAR in order to calculate more accurately flows with high non-condensable mass fractions. To be able to take into account this kind of flow with system code is crucial for safety analysis, especially in

specific situations such as accident scenarios occurring during mid-loop operations in cold shutdown states.

- Based on a physical approach from the literature, this new model enables to better qualify the gas-liquid interface vapour composition and temperature in order to assess the interfacial heat transfer correctly. Some validation elements are given in the present paper, but an extensive study of this approach is still under way and will be specifically addressed.

- The new model also helps improving the code numerical stability. By no longer estimating interface temperature close to 0°C in case of low vapour concentration in the gas phase, fluid property evaluation remains in the code available tabulation and calculation can run in a smoother way.

- It is now possible to investigate reactor cold-shutdown study, while it was difficult with ASTEC previous versions. Results provided in the paper constitute a feasibility study and show that both the complete cold shutdown sequence of the reactor and a first example of an accidental event can be calculated in ASTEC with a reasonable calculation time and no major numerical issues encountered. This first calculation study does not discuss the results validity as it should be done through further work but aims at showing new investigation fields possible with ASTEC.

Nomenclature

A_i	Interfacial area (m^{-1})
Cp	Heat capacity at constant pressure ($J.kg^{-1}.K^{-1}$)
D	Flow characteristic length (m)
$\mathcal{D}$	Diffusivity coefficient ($m^2.s^{-1}$)
f	Molar fraction (-)
h	Heat transfer coefficient ($W.m^{-2}.K^{-1}$)
K	Mass transfer coefficient ($m.s^{-1}$)
L	Latent heat ($J.kg^{-1}$)
$\dot{m}$	Mass flow rate ($kg.s^{-1}$)
P	Pressure (Pa)
Q	Heat transfer (W)

T	Temperature (K)
V	Volume (m^3)
X	Mass fraction (-)

Greek symbols

α	Void fraction (-)
ρ	Density ($kg.m^{-3}$)
λ	Thermal conductivity ($W.m^{-1}.K^{-1}$)
μ	Dynamic viscosity (Pa.s)

Adimensional numbers

Nu	Nusselt number $\left(\frac{\square D}{\lambda}\right)$
Pr	Prandtl number $\left(\frac{\mu C_p}{\lambda}\right)$
Sc	Schmidt number $\left(\frac{\mu}{\rho \mathcal{D}}\right)$
Sh	Sherwood number $\left(\frac{KD}{\mathcal{D}}\right)$

Subscripts

cond	Condensation
diff	Diffusion
g	Gas
i	Interfacial
in	At inlet
inj	Injected
k	Phase
l	Liquid
NC	Non-condensable

sat	Saturation
tot	Total
v	Vapour
vap	Vaporisation

Acronyms

CCWS	Component cooling water system
CVCS	Chemical and volume control system
LOCA	Loss of coolant accident
NP	Nominal power
PWR	Pressurised water reactor
RCS	Reactor coolant system
RHR	Residual heat removal

5. References

[1] D.F. Othmer, "The condensation of steam", Industrial and Engineering Chemistry, Vol. 21, No. 6, 1929, pp. 576-583.

[2] J. Huang, J. Zhang and L. Wang "Review of vapor condensation heat and mass transfer in the presence of non-condensable gas", Applied Thermal Engineering, Vol. 89, 2015, pp. 469-484.

[3] B. Ren, L. Zhang, J. Cao, H. Xu and Z. Tao, "Experimental and theoretical investigation on condensation inside a horizontal tube with noncondensable gas", International Journal of Heat and Mass Transfer, Vol. 82, 2015, pp. 588-603.

[4] Y-S. Son and J-Y. Shin, "Thermal-hydraulic analysis on the effect of operator action in the loss of shutdown cooling system accident in a PWR", Nuclear Engineering and Design, Vol. 237, 2007, pp. 2054-2063.

[5] D. Dumont, G. Lavialle, B. Noel and R. Deruaz, "Loss of residual mid-loop operation: BETHSY experiments", Nuclear Engineering and Design, Vol. 149, 1994, pp. 365-374.

[6] J. Gou, H. Ma, Z. Yang and Y. Shan, "Analysis of loss of residual heat removal system for CPR1000 under cold shutdown operation", Annals of Nuclear Energy, Vol. 105, 2017, pp. 25-35.

[7] N. Aksan, "An overview on thermal-hydraulic phenomena for water cooled nuclear reactors; part I: SETs, and ITFs of PWRs, BWRs, VVERs", Nuclear Engineering and Design, Vol. 354, 2019, 110212.

[8] L. Chailan, A. Bentaïb, P. Chatelard, "Overview of ASTEC code and models for Evaluation of Severe Accidents in Water Cooled Reactors", Proceedings of IAEA

Technical Meeting on Status and Evaluation of Severe Accident Simulation Codes for Water Cooled Reactors, Vienna (Austria), October 9-12, 2017

[9] T. Kageyama, P. F. Peterson and V. E. Schrock, “Diffusion layer modeling for condensation in vertical tubes with noncondensable gases”, Nuclear Engineering and Design, Vol. 141, 1993, pp. 289-302.

[10] J. M. Yoo, J. H. Kang, B. J. Yun, S. W. Hong and J. J. Jeong, “Improvement of the MELCOR condensation heat transfer model for the thermal-hydraulic analysis of a PWR containment”, Progress in Nuclear Energy, Vol. 104, 2018, pp. 172-182.

[11] J-Y. Lee, J. J. Jeong, J-H. Kang and B. Yun, “Improvement of the condensation heat transfer model of the MARS-KS1.3 code using a modified diffusion layer model”, Progress in Nuclear Energy, Vol. 108, 2018, pp. 260-269.

[12] P. Coste and D. Bestion, “A simple modelling of mass diffusion effects on condensation with noncondensable gases for the Cathare code”, NURETH 7, Saratoga Springs, NY (United States), September 10-15th 1995.

[13] A. Janicot and D. Bestion, “Condensation modelling for ECC injection”, Nuclear Engineering and Design, Vol. 145, 1993, pp. 37-45.

[14] A. Tanrikut and O. Yesin, “Experimental research on in-tube condensation in the presence of air”, Proceedings of a Technical Committee Meeting, IAEA TECDOC-1149, Switzerland, 1998, pp. 14-17.

[15] G. Bandini, M. Buck, W. Hering, L. Godin-Jacqmin, G. Ratel, P. Matejovic, M. Barnak, G. Paitz, A. Stefanova, N. Trégourès, G. Guillard and V. Koundy, “Recent advances in ASTEC validation on circuit thermal-hydraulic and core degradation”, Progress in Nuclear Energy, Vol. 52, 2010, pp. 148-157.

[16] T. Glantz, T. Taurines, O. de Luze, S. Belon, G. Guillard and F. Jacq, “DRACCAR: A multi-physics code for computational analysis of multi-rod ballooning , coolability and fuel relocation during LOCA transients Part one: General modelling description”, Nuclear Engineering and Design, Vol. 339, 2018, pp. 269-285.

[17] I. Gómez-García-Toraño, L. Laborde, "Validation of the CESAR friction models of the ASTECV21 code based on Moby Dick experiments”. Journal of Nuclear Engineering and Radiation Sciences. 5, 2019. 1–9. https://doi.org/10.1115/1.4042119.